JACS
JOURNAL OF THE AMERICAN CHEMICAL SOCIETY
Article
pubs.acs.org/JACS

Mechanism for the Direct Synthesis of H_2O_2 on Pd Clusters: Heterolytic Reaction Pathways at the Liquid–Solid Interface

Neil M. Wilson and David W. Flaherty*

Department of Chemical and Biomolecular Engineering University of Illinois Urbana–Champaign, Urbana, Illinois 61801, United States

Supporting Information

ABSTRACT: Direct synthesis ($H_2 + O_2 \rightarrow H_2O_2$) is a promising reaction for producing H_2O_2, which can replace chlorinated oxidants in industrial processes. The mechanism of this reaction and the reasons for the importance of seemingly unrelated factors (e.g., Pd cluster size and solvent pH) remain unclear despite significant research. We propose a mechanism for H_2O_2 formation on Pd clusters consistent with steady-state H_2O_2 and H_2O formation rates measured as functions of reactant pressures and temperature and the interpretations of proton concentration effects. H_2O_2 forms by sequential proton–electron transfer to O_2 and OOH surface intermediates, whereas H_2O forms by O–O bond rupture within OOH surface species. Direct synthesis, therefore, does not proceed by the Langmuir–Hinshelwood mechanism often invoked. Rather, H_2O_2 forms by heterolytic reaction pathways resembling the two-electron oxygen reduction reaction (ORR); however, the chemical potential of H_2 replaces an external electrical potential as the thermodynamic driving force. Activation enthalpies ($\Delta H^{\ddagger}$) for H_2O formation increase by 14 kJ mol^{-1} when Pd cluster diameters increase from 0.7 to 7 nm because changes in the electronic structure of Pd surface atoms decrease their propensity to cleave O–O bonds. $\Delta H^{\ddagger}$ values for H_2O_2 remain nearly constant because barriers for proton–electron transfer depend weakly on the coordinative saturation of Pd surface atoms. Collectively, these results provide a self-consistent mechanism, which clarifies many studies in which H_2O_2 rates and selectivities were shown to depend on the concentration of acid/halide additives and Pd cluster size. These findings will guide the rational design of selective catalysts for direct synthesis.

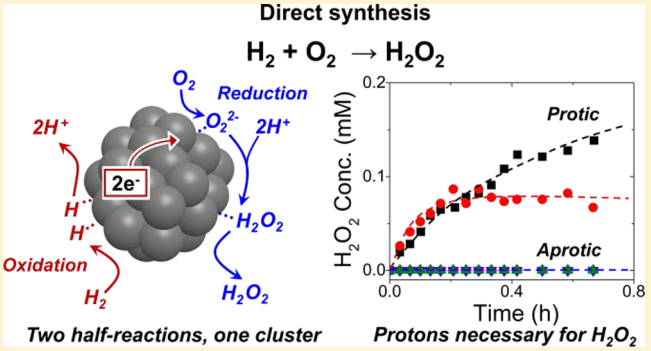

1. INTRODUCTION

Hydrogen peroxide (H_2O_2) is an effective and environmentally benign alternative to chlorinated oxidizers (e.g., HClO and ClO_2) commonly used to selectively oxidize organic molecules (e.g., propylene), bleach pulp and paper, and treat wastewater.[1] The primary byproducts of the reactions between H_2O_2 and organic compounds are H_2O and O_2; therefore, H_2O_2 is an appealing oxidant, which unlike chlorinated oxidizers does not produce toxic chloroform, dioxins, and polychlorinated hydrocarbons.[2,3] However, the current market cost of H_2O_2 is not competitive with chlorinated oxidizers because the dominant method for H_2O_2 production (anthraquinone auto-oxidation (AO))[1] inherently requires energy-intensive separation and concentration steps, and thus has high capital and operating costs. For H_2O_2 to be more widely used, costly separation steps must be eliminated;[4] therefore, its production cannot involve anthraquinones. Rather, H_2O_2 needs to be produced by a radically different catalytic chemistry.

The direct synthesis of H_2O_2 ($H_2 + O_2 \rightarrow H_2O_2$) appears to be the most promising alternative to AO.[4,5] Direct synthesis does not involve organic substrates (i.e., anthraquinones), uses greener solvents (e.g., H_2O, CH_3OH), and consequently requires fewer separation steps and much less energy to produce H_2O_2.[4,6] Direct synthesis, however, suffers from low H_2O_2 selectivity because significant amounts of H_2O form by primary and secondary reactions that irreversibly cleave the O–O bond[7] of surface intermediates chemisorbed on transition metal cluster catalysts.[5,8−11] The greatest H_2O_2 selectivities are achieved on catalysts that cleave O–O bonds at low rates[12,13] but add hydrogen to O_2* at high rates.[10] Pd catalysts have higher H_2O_2 selectivities (60–75%) than Pt catalysts (5–20%)[14] and give H_2O_2 formation rates nearly 100-fold greater than those for Au.[15,16] Yet Pd only gives such high selectivities in strongly acidic solvents (e.g., ethanol, 0.12 M H_2SO_4)[14] containing halides (e.g., Cl^-, Br^-), which modify the reactivity of the Pd surfaces in ways not fully understood.[14,17−20] Researchers must develop catalysts that give greater selectivities toward H_2O_2 without the need for solvents containing mineral acids and halides in order for direct synthesis to be more viable.[1,19]

Rational design of such catalysts require fundamental, molecular-level knowledge of the mechanism for H_2O_2 formation on metal clusters; however, the direct synthesis reaction is poorly understood. H_2O_2 formation rates on Pd

Received: October 12, 2015
Published: November 23, 2015

DOI: 10.1021/jacs.5b10669
J. Am. Chem. Soc. 2016, 138, 574–586

Table 1. Characterization Results for Pd Catalysts

sample	Pd content (% wt)[a]	temperature (K)		$\langle d_{CHEM}\rangle$ (nm)[d]	$\langle d_{TEM}\rangle$ (nm)[e]
		oxidative treatment[b]	reductive treatment[c]		
0.7 nm Pd−SiO_2	0.05	n/a	573, 4 h	0.7	n/a
3 nm Pd−SiO_2	0.04	673, 4 h	573, 4 h	3	4 ± 1
7 nm Pd−SiO_2	0.05	973, 4 h	573, 4 h	7	7 ± 1
3.8 wt % Pd−SiO_2	3.8	n/a	573, 4 h	n/a	5 ± 1

[a]Metal content of samples determined by inductively coupled plasma optical emission spectroscopy following digestion in a 2:1 volume ratio of HNO_3 (Fisher Scientific, 67−70 wt %) to HF (Fisher Scientific, 48−51 wt %) [b]100 cm^3 min^{-1} dry air. [c]20 kPa H_2, 81 kPa He, 100 cm^3 min^{-1}. [d]Average cluster diameter determined by CO chemisorption ($\langle d_{chem}\rangle$) was calculated using total CO uptake obtained over the range of 0.03−0.4 kPa CO at 303 K with the assumption of hemispherical clusters and an adsorption stoichiometry of two Pd_s to one CO molecule.[39,40] [e]Surface-averaged mean cluster diameter from transmission electron microscopy analysis using $\langle d_{TEM}\rangle = (\Sigma_i n_i d_i^3/\Sigma_i n_i d_i^2)$ of >100 clusters.

clusters depend strongly on several seemingly disparate factors including the pH of the solvent,[21−23] the presence (or absence) of halide coadsorbates,[22−25] and the size of the metal clusters.[26,27] The manner by which these factors collectively determine H_2O_2 selectivities and rates have not been resolved in previous studies. Protons (H^+) have been suggested to affect surface chemistry through indirect (i.e., electronic interactions)[21] or by directly participating in O_2 reduction.[24,28] The additions of mineral acids (e.g., HCl,[21,29] H_2SO_4,[14,21] H_3PO_4,[22,24] and HNO_3)[22] to solvents for direct synthesis increase the concentrations of H^+ and H_2O_2 selectivities, but they also introduce strongly binding anions (e.g., Cl^-, SO_4^{2-}, PO_4^{3-}, and NO_3^-) that modify the electronic structure of metal clusters directly. To the best of our knowledge, there are no direct measurements that implicate H^+ in the direct synthesis of H_2O_2. The addition of halides to Pd clusters in acidic ethanol (0.12 M H_2SO_4) increases H_2O_2 selectivities from 60 to 80%.[21] These changes have been attributed to halide adsorption either blocking sites that promote O−O bond scission[12,24,30,31] or reducing the density of states near the Fermi level and consequently making metal surfaces less reactive for O−O cleavage.[31−35] H_2O_2 selectivities do increase when halides and acids are added to solvents for direct synthesis, yet these species are difficult to remove from the product stream. As such, there is significant interest in using other strategies to achieve high selectivities including alloying Pd with other metals (e.g., Au)[8,19] and controlling the size of the Pd clusters.[26,27] PdAu alloy nanoclusters supported on carbon give H_2O_2 selectivities (80%) much greater than those on Pd (42%) and H_2O_2 formation rates 100 times larger than those on Au.[19] In addition, studies over a narrow range of Pd cluster sizes (3.4−4.2 nm) on SiO_2 show that H_2O_2 selectivity increases modestly with increasing cluster size.[27] The mechanisms by which alloying or changes in the cluster size affect H_2O_2 selectivities remain unknown but are likely related to either ensemble effects (e.g., decreased number of sites that rupture O−O bonds)[12,36] or electronic effects (e.g., reduced electron back-donation from Pd into π^* orbitals of the O−O bond).[26,32] The uncertain explanations for the effects of acids and cluster size as well as the poorly understood connections between these factors and the mechanism for H_2O_2 formation impede rational design of improved catalysts for direct synthesis.

In this study, we propose a mechanism for direct synthesis of H_2O_2 on Pd clusters that is consistent with our measurements and with previously published observations and that provides guiding principles for the design of metal catalysts that will give greater selectivities and formation rates for H_2O_2. Here, we report steady-state H_2O_2 and H_2O formation rates on Pd clusters (0.7−7 nm) and their dependence on the pressure of H_2 (5−400 kPa) and O_2 (25−400 kPa), the protic or aprotic nature of the reaction solvent, and the concentration and identity of proton donors over a range of relevant temperatures (273−305 K). Formation rates of both H_2O_2 and H_2O are sensitive to the H_2 pressure but show no dependence on the O_2 pressure. H_2O_2 selectivities and formation rates require that H^+ are present in the solvent and increase slightly with the addition of H^+ donors (e.g., H_2SO_4, HCl, or H_2CO_3), whereas rates for H_2O_2 formation are immeasurable (>10^3 times lower) in aprotic solvents. Collectively, these rate measurements are inconsistent with previously proposed Langmuirian reaction mechanisms. Instead, these data show that H_2O_2 is formed by kinetically relevant proton (from solvent molecules)—electron (provided by heterolytic hydrogen oxidation, $H_2 \leftrightarrow 2H^+ + 2e^-$) transfer to hydroperoxy surface intermediates. This mechanism resembles that for the two-electron oxygen reduction reaction (ORR);[37] however, both half-reactions occur on a single Pd cluster in the absence of an electrical potential. Rather, gaseous H_2 provides a chemical potential which drives O_2 reduction. These mechanistic conclusions agree also with measured activation enthalpies ($\Delta H^{\ddagger}$) and the differences among their values on 0.7, 3, and 7 nm Pd clusters. Values of $\Delta H^{\ddagger}$ for H_2O_2 formation rates remain nearly constant (9−14 kJ mol^{-1}) as the mean size of the Pd clusters increase; however, $\Delta H^{\ddagger}$ for H_2O formation increases noticeably (18 to 32 kJ mol^{-1}). These comparisons show that processes that form H_2O_2 (proton−electron transfer) are less sensitive to changes in the electronic structure of Pd surfaces than those that create H_2O (i.e., O−O bond dissociation), which is consistent with prior research of the ORR and our mechanistic conclusions. The data and interpretations suggest that greater H_2O_2 selectivities can be achieved when metal clusters, which heterolytically dissociate H_2 and bind O_2 tightly enough to facilitate electron transfer, contact solvents with high H^+ concentrations. These findings will guide the development of productive catalysts for the direct synthesis of H_2O_2 and help to advance the use of H_2O_2 for the production of commodity chemicals.

2. MATERIALS AND METHODS

2.1. Synthesis of Supported Pd Catalysts. Pd catalysts were prepared by strong electrostatic adsorption (SEA) of Pd precursors onto silica,[38] followed by oxidation and reduction to form metallic clusters. All gases used were 99.999% pure and supplied by S. J. Smith Co. unless otherwise stated. Silica (15 g, Sigma-Aldrich, Davisil 646, 35−60 mesh) was added to 300 cm^3 of deionized (DI) water (17.8 MΩ) followed by the addition of 30 cm^3 of 14.5 M NH_4OH (Macron, 28−30 wt %) in order to obtain a solution pH greater than 11. In a separate beaker, 17.4 mg of $Pd(NH_3)_4Cl_2$ (Sigma-Aldrich, ≥99.99%) was added to 15 cm^3 of DI water; subsequently, this solution was added to the basic solution containing silica. The resulting solution was stirred for 3 h and then

DOI: 10.1021/jacs.5b10669
J. Am. Chem. Soc. 2016, 138, 574−586

vacuum filtered to recover the solids. The wet solids were rinsed with an additional 500 cm^3 of DI water, vacuum filtered, and then allowed to dry. The dried solids were heated to 573 K at 3 K min^{-1} and then held at 573 K for 4 h in a flowing mixture of 20 kPa H_2 and 81 kPa He (100 cm^3 min^{-1}) with the intent to reduce the Pd to metallic nanoclusters. Oxidative treatments in flowing dry air (Table 1) were used after the initial reduction to increase the average size of the Pd clusters. These were followed by a second reductive treatment (573 K, 4 h, 20 kPa H_2, 81 kPa He, 100 cm^3 min^{-1}) to form metallic Pd nanoclusters. After reduction, all samples were passivated at ambient temperature by exposure to a flowing (500 cm^3 min^{-1}) mixture of 4 kPa O_2 and 97 kPa He for 0.5 h.

A 3.8 wt % Pd−SiO_2 catalyst was prepared by incipient wetness impregnation of 200 mg of washed SiO_2 with 0.21 cm^3 of 0.45 M K_2PdCl_4 (Sigma-Aldrich, 99.99%). The catalyst was then dried under ambient conditions for 4 h before reduction and passivation treatments identical to those described above.

2.2. Mean Pd Cluster Sizes and Metal Loading. The average diameters of clean Pd clusters were estimated from the volumetric uptake of CO ($<d_{CHEM}>$) and from cluster size distributions obtained by transmission electron microscopy (TEM). Volumetric CO uptakes were measured at 303 K using a custom-built borosilicate-glass chemisorption cell. Loaded catalysts were degassed by heating to 323 K at 3 K min^{-1} and holding for 12 h while evacuating the system with a turbo pump (Edwards, EXT250), after which the sample was cooled and the cell was checked for leaks. Samples were then treated in flowing H_2 (50 cm^3 min^{-1}) while heating to 523 K at 3 K min^{-1} and holding at 523 K for 0.5 h. The sample was then evacuated at 523 K for 0.5 h using the turbo pump, and the cell was allowed to cool to 303 K under dynamic vacuum. The total amount of CO (S.J. Smith, 99.99%) adsorbed onto the Pd clusters within each sample was determined by measuring volumetric uptakes between 0.03 and 0.4 kPa and extrapolating the linear portion of the isotherm to zero pressure. The number of exposed Pd atoms (Pd_s) was determined by assuming a ratio of two Pd_s to one CO molecule.[39,40] The mean cluster diameter for each sample was estimated from Pd_s and the total Pd loading by assuming a hemispherical geometry and an atomic radius of 0.14 nm for Pd.

The distribution of cluster diameters was measured by bright-field TEM imaging (JEOL 2010 LaB_6) of more than 100 clusters. Samples were prepared by grinding the catalyst to a fine powder (<200 mesh), which was then suspended in ethanol (Decon Laboratories Inc., 100%) by gentle stirring and loaded onto a Cu holey-carbon TEM grid (200 mesh, Ted Pella Inc.). The wet grids were dried under ambient conditions for at least 4 h. The surface area normalized average cluster diameter ($<d_{TEM}>$) for each catalyst was calculated using

$$<d_{TEM}> = \frac{\sum_i n_i d_i^3}{\sum_i n_i d_i^2} \quad (1)$$

where n_i is the number of clusters with diameter d_i. Figure 1 shows a representative TEM image of the 7 nm Pd clusters, with the cluster diameter distribution as inset, and TEM images for the other Pd catalyst are given in Figure S1.1. The diameters of the clusters formed using only reductive treatments were too small (<1 nm) to be measured accurately by TEM. The values of $<d_{TEM}>$ and $<d_{CHEM}>$ agree closely for the 3 and 7 nm Pd clusters. The Pd content of each sample was measured by inductively coupled plasma optical emission spectroscopy (PerkinElmer, Optima 2000DV). The characterization results for all prepared catalysts are shown in Table 1.

2.3. Steady-State H_2O_2 and H_2O Formation Rate Measurements. Steady-state reaction rates were measured using a packed-bed, continuous-flow reactor (0.32 cm I.D., 11 cm long) contained within a stainless-steel cooling jacket (3.8 cm O.D.). The reactor was loaded with 150−300 mg of Pd−SiO_2, which was held between plugs of glass wool (6−10 mg), each supported by borosilicate glass rods (2 mm diameter). These, in turn, were secured between silver-coated fritted VCR gaskets (Swagelok, SS-4-VCR-2-60M), which were also used to seal the reactor to the tubing of the gas−liquid handling manifold. The temperature of the reactor (273−305 K) was controlled by flowing aqueous ethylene glycol through the cooling jacket using a refrigerated recirculating bath

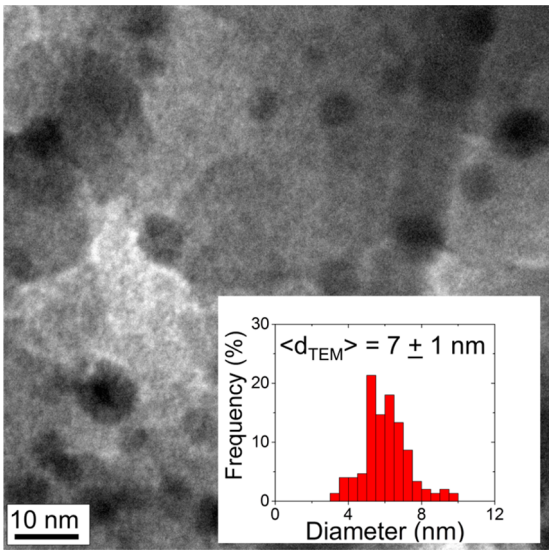

Figure 1. Representative TEM image of the 7 nm Pd−SiO_2 catalyst with cluster size distribution (inset). More than 100 clusters were measured to determine the value of $<d_{TEM}>$, the surface area averaged diameter.

(Neslab, Endocal). The temperature of the catalyst bed was monitored directly using a K-type thermocouple contained within the cooling jacket and in firm contact with the stainless-steel wall surrounding the catalyst bed. Certified reactant gas mixtures (25% H_2, balance N_2, and 5% O_2, balance N_2; or 5% H_2, balance N_2, and 25% O_2, balance N_2) and CO_2 (S.J. Smith, 99.99%) were introduced to the system upstream of the catalyst bed using digital mass-flow controllers (MFC; Porter, 601 series). Gas mixtures were chosen to contain sufficient N_2 to ensure that flammable mixtures of H_2 and O_2 never formed.[41] The reaction solvent (aqueous CH_3OH (Macron, ≥ 99.8%) solutions, 20−100% v/v) were introduced to the system downstream of the MFCs using a high-performance liquid chromatography (HPLC) pump (Waters, 515). The molecular species used to control the pH of the solution (H_2SO_4 (Macron, 95−98%), H_3PO_4 (Fisher Scientific, 88.9%), HCl (Macron, 36.5−38%), and $NaHCO_3$ (Fisher Scientific, > 99.7%)) were combined with the solvent within the HPLC pump reservoir, and the solvent pH was measured with a digital pH meter (Omega, PHH22). The gas and liquid streams contacted and mixed within 120 cm of 1.6 mm I.D. tubing before flowing through the catalyst bed in an upflow configuration. The reactor pressure (0.1−3.1 MPa) was controlled using an electronic pressure reducer (EPR; Proportion Air, QB1S) and a back-pressure regulator (BPR; Equilibar, EB1LF1-SS316) equipped with a Kapton diaphragm. The pressure at the inlet of the reactor was measured with a digital pressure gauge (Omega, DPG8001-1K), and the pressure at the reactor outlet was monitored using the EPR.

The collection and characterization of the liquid and gaseous effluent streams was automated and operated continuously. The liquid and gaseous portions of the reactor effluent were separated using an acrylic gas−liquid separator (GLS) located downstream of the BPR. The gas stream passed through a check valve (Swagelok, 1.7 kPa cracking pressure) before flowing into the automated gas sampling valve for a gas chromatograph (Agilent, 7890). The components of the gas stream were separated using a packed column (Sigma-Aldrich, 3 m length × 2.1 mm ID, Molecular Sieve 5A) and their concentrations were analyzed using a thermal conductivity detector. Ar was used as both the carrier and reference gas during gas chromatography. Liquid samples were withdrawn from the GLS using an automated valve (Vici, 10 port valve), which was configured to inject 0.4 cm^3 of the effluent liquid and also 1 cm^3 of a colorimetric indicator solution (12 mM neocuproine, Sigma-Aldrich, ≥ 98%; 8.3 mM $CuSO_4$, Fisher Scientific, ≥ 98.6%; 25% v/v ethanol, Decon Laboratories Inc., 100%)[42] into glass vials held within an automated fraction collector (Biorad, 2110). The concentration of H_2O_2 in each vial was determined from its absorbance at 454 nm, measured using a spectrophotometer (Spectronic, 20 Genesys). The absorbance

DOI: 10.1021/jacs.5b10669
J. Am. Chem. Soc. 2016, 138, 574−586

values were calibrated using solutions of known colorimetric indicator solution with known H_2O_2 concentrations.

Primary rates of H_2O_2 and H_2O formation were measured by avoiding artifacts introduced by mass transport limitations and uncertainties from secondary H_2O_2 decomposition. To ensure that the Madon–Boudart criterion[43] was satisfied, H_2 conversion was measured as a function of gas residence time ((mol Pd_s s) (mol H_2)$^{-1}$) on catalysts with different metal loadings (0.025–0.5 wt %) at high H_2 pressure (400 kPa H_2) where H_2O_2 and H_2O formation rates were the greatest (Figure S2.1). The H_2 conversion at a given gas residence time did not depend on metal loading for catalysts with Pd contents ≤0.05 wt %, indicating that intrapellet mass transport limitations did not exist in this range of metal loading. H_2O_2 formation rates were measured as a function of liquid residence time (2.1–4.2 s) over a range of temperatures (266–305 K) to examine the significance of secondary decomposition of H_2O_2 (Figure S2.2). The H_2O_2 formation rate depended strongly on the liquid residence time at temperatures greater than 281 K, indicating significant secondary decomposition of H_2O_2. Mass transport restrictions and secondary decomposition of H_2O_2 were avoided throughout this study by using 0.05 wt % Pd catalyst, a solvent flow rate of 10 cm^3 min^{-1}, and a reaction temperature of 277 K unless otherwise stated. The catalyst was changed after each data set, typically on a daily basis, which prevented slow leaching of the Pd from affecting the rate measurements significantly. After the catalyst was loaded, it was allowed to stabilize for at least 6 h under reaction conditions prior to data collection. Data was collected for at least 1.5 h under each set of conditions to acquire multiple rate measurements at steady state. Reported rates comprise the mean values of at least six measurements, and error bars represent the standard deviation of these measurements.

2.4. Rate Measurements in Semibatch Reactors. H_2O_2 formation rates were measured in protic and aprotic solvents using a 60 cm^3 borosilicate glass semibatch reactor (43.5 mm I.D.). The reactant gases entered through a fine glass frit at the bottom of the reactor and were highly dispersed as they rose up through a turbulent suspension of the catalyst and the solvent. The outlet at the top of the reactor was made to be 3.5 mm I.D. to decrease the rate of solvent loss during each experiment. The reactor was filled with 40 cm^3 of either pure DI water (17.8 MΩ), methanol (Macron, ≥99.8%), acetonitrile (Fisher Scientific, 99.9%), dimethyl sulfoxide (Fisher Scientific, 99.9%), or propylene carbonate (Sigma-Aldrich, 99.7%), which were all used as received. The reactant gas mixture (4.2 kPa H_2, 4.2 kPa O_2, balance N_2) was introduced at a total flow rate of 60 cm^3 min^{-1} and controlled using variable area rotameters (Omega, FL-1461-S). The 3.8 wt % Pd–SiO_2 catalyst (20 mg) was added to the reactor to initiate the reaction after the gas flow rate became stable. Liquid samples (0.4 cm^3) were taken every 2–5 min in order to measure the concentration of H_2O_2 by the colorimetric titration procedure described earlier (section 2.3), and the reaction was conducted at ambient temperature (~295 K). The SEA-prepared Pd catalysts were not used in the semibatch reactor because the long Pd–liquid contact times (46 s g_{Pd} L^{-1} compared to 1.5×10^{-2} s g_{Pd} L^{-1} in the plugged-flow reactor) caused significant amounts of Pd to leach into the solution. Control experiments showed that these dissolved Pd species interact with and perhaps oxidize the colorimetric titrant so that the H_2O_2 concentration could not be measured accurately. Therefore, the semibatch experiments were conducted using the 3.8 wt % Pd–SiO_2 catalyst prepared by incipient wetness impregnation (section 2.1), which contains trace amounts of Cl that may reduce leaching.

3. RESULTS AND DISCUSSION

3.1. Dependence of Rates on Reactant Pressures and Mechanistic Interpretation. Figure 2 shows turnover rates for the formation of H_2O_2 (Figure 2a) and H_2O (Figure 2b) from the reduction of O_2 on 0.7 nm Pd clusters as a function of H_2 pressure (5–400 kPa H_2, 60 kPa O_2, 277 K) and O_2 pressure (25–400 kPa O_2, 60 kPa H_2, 277 K). The H_2O_2 and H_2O formation rates do not depend on O_2 pressure (((O_2))), likely because the reactive surface sites are saturated with O_2-derived

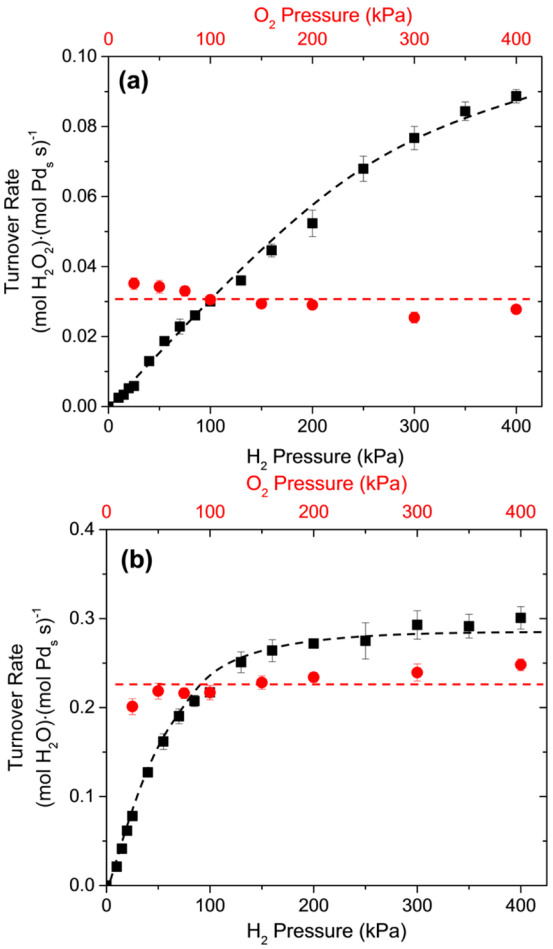

Figure 2. (a) H_2O_2 and (b) H_2O turnover rates as functions of H_2 pressure at 60 kPa O_2 (black, ■) and O_2 pressure at 60 kPa H_2 (red, ●) on 0.7 nm Pd clusters (277 K, 10 cm^3 min^{-1} CH_3OH). Lines are intended to guide the eye.

intermediates such as O_2** (where ** and * denote η^2 and η^1 adsorbed Pd surface intermediates, respectively) or hydroperoxy (OOH**) over the full range of (O_2) tested here (25–400 kPa). This interpretation is consistent with high heats of adsorption for molecular oxygen onto H_2O-saturated Pd (48–75 kJ mol^{-1})[10,44] and Pt (39–47 kJ mol^{-1})[45,46] surfaces (i.e., $2H_2O^* + O_2 \rightarrow O_2^{**} + 2H_2O$) even within liquid water. Presumably, reactive sites on Pd surfaces would be covered by H_2O^* and rates would depend on the value of (O_2) at sufficiently low (O_2). Calculated changes in the Gibbs free energy for H_2O^* displacement by O_2 (−39 kJ mol^{-1})[45] suggest, however, that metal surfaces are covered by O_2** even at pressures orders of magnitude less than the lowest (O_2) tested here (25 kPa O_2; Supporting Information section S3).

Figure 2 shows that the formation rates of H_2O_2 and H_2O depend strongly on H_2 pressure ((H_2)), even though they do not change with (O_2). The H_2O_2 formation rate initially increases linearly with (H_2) from 5 to 150 kPa (Figure 2a) and reaches a half-order dependence on (H_2) (i.e., $r_{H_2O_2} \sim (H_2)^{1/2}$) at partial pressures near 400 kPa. Under these same conditions, H_2O turnover rates are proportional to $(H_2)^{1/2}$ between 5 and 150 kPa and become constant at greater pressures (Figure 2b). These data (Figure 2a) are consistent with the previously reported first-order dependence of H_2O_2 formation rates on (H_2), measured from 5 to 24 kPa H_2 on silica supported Pd clusters,[21] yet that

DOI: 10.1021/jacs.5b10669
J. Am. Chem. Soc. 2016, 138, 574–586

work did not observe changes in the (H_2) dependence over the small range of pressures tested. Mechanistic interpretations of those results could not disprove or prove any of the proposed mechanisms for H_2O_2 formation,[10,11,28,47] in part because the range of H_2 pressures was limited but also because formation rates for H_2O were not reported.

H_2O_2 and H_2O formation rates depend on the prevalent H_2 and O_2 pressures because changes in the partial pressure of the reactants change either the concentrations of species involved in kinetically relevant steps, the identity of the most abundant reactive intermediates (MARI) or both.[32] The data shown in Figure 2 implies that the reactive sites are saturated with O_2-derived intermediates whose composition changes as (H_2) increases. Oxygen isotope labeling experiments show that H_2O_2 cannot be formed once the O−O bond of molecular O_2 cleaves;[7] therefore, the rate data (Figure 2), together with this observation, suggest that the MARI may be a species that contains an intact O−O bond (i.e., O_2**, OOH**, or H_2O_2**). The saturation of metal surfaces by such intermediates is consistent with in situ infrared spectroscopy studies showing large coverages of O_2** on Pt during the ORR at low potentials[48] and interpretations of the effects of anions and bromide on ORR rates.[49−51] In addition, the dependence of both H_2O_2 and H_2O formation rates on (H_2) shows that H_2-derived intermediates participate in the kinetically relevant steps that form each product. Finally, the simultaneous changes in the dependence of H_2O_2 and H_2O formation rates on (H_2) at ∼150 kPa H_2 suggest that the average composition of the MARI increases by a single H atom.

Langmuir−Hinshelwood mechanisms proposed for H_2O_2 formation,[10,11,47] which involve direct reduction of O_2** by sequential reactions with H* atoms bound to adjacent surface sites, fail to describe these data (Figure 2). Specifically, such mechanisms predict H_2O_2 formation rates that are independent of (H_2), depend inversely on (O_2), or have a first-order dependence on (O_2) depending on the identity of the MARI (derivation, Supporting Information section S4), which are inconsistent with measured reaction rates (Figure 2a). A two-site Langmuirian model, which involves distinct sites for O_2 and H adsorption could describe the data in Figure 2 (Supporting Information section S5); however, it would require that the sites capable of binding H* atoms remain empty over the entire range of H_2 pressures (5−400 kPa). This assumption seems unlikely because the heat of adsorption of a H atom on Pd (72 kJ mol^{-1}) from calculated energies of H adsorption on Pd at low H coverage[52] and the homolytic bond dissociation energy of H_2[53] is significantly higher than that for H_2O on Pd(111) (39 kJ mol^{-1}).[52] Additional evidence, which shows that H_2O_2 forms only in protic solvents (section 3.2), further suggests that this reaction occurs by a non-Langmuirian mechanism. Thus, H_2O_2 appears to form by pathways that involve reactive intermediates not present on the surface of Pd clusters.

Scheme 1 shows a proposed series of elementary steps that are consistent with the effects of H_2 and O_2 pressure on product formation rates on Pd clusters (Figure 2) and on other transition metal clusters[21,47,54] within liquid solvents. These steps involve bimolecular reactions between liquid-phase species, namely H^+, and chemisorbed surface intermediates. Dissociative H_2 adsorption (Scheme 1, step 1) and heterolytic H* oxidation (Scheme 1, step 2) steps as well as molecular adsorption of O_2 (Scheme 1, step 3) and desorption of H_2O_2 (Scheme 1, step 6) and H_2O (Scheme 1, step 11) are assumed to be quasi-equilibrated under all conditions. These assumptions are based on free energies for O_2 and H_2 adsorption that become negligible

Scheme 1. Proposed Series of Elementary Steps for H_2O_2 and H_2O Formation during Direct Synthesis on Supported Pd Clusters[a]

$$H_2 + 2* \underset{k_{-1}}{\overset{k_1}{\rightleftharpoons}} 2H* \quad (1)$$

$$H* \underset{k_{-2}}{\overset{k_2}{\rightleftharpoons}} H^+ + e^- + * \quad (2)$$

$$O_2 + ** \underset{k_{-3}}{\overset{k_3}{\rightleftharpoons}} O_2** \quad (3)$$

$$O_2** + H^+ + e^- \underset{k_{-4}}{\overset{k_4}{\rightleftharpoons}} OOH** \quad (4)$$

$$OOH** + H^+ + e^- \xrightarrow{k_5} H_2O_2** \quad (5)$$

$$H_2O_2** \underset{k_{-6}}{\overset{k_6}{\rightleftharpoons}} H_2O_2 + ** \quad (6)$$

$$O_2** \xrightarrow{k_7} 2O* \quad (7)$$

$$OOH** \xrightarrow{k_8} OH* + O* \quad (8)$$

$$O* + H* \xrightarrow{k_9} OH* + * \quad (9)$$

$$OH* + H* \xrightarrow{k_{10}} H_2O* + * \quad (10)$$

$$H_2O* \underset{k_{-11}}{\overset{k_{11}}{\rightleftharpoons}} H_2O + * \quad (11)$$

$$H_2O_2** \xrightarrow{k_{12}} 2OH* \quad (12)$$

[a]* denotes an empty site, X* represents an adsorbate bound to a single Pd atom, X** signifies an intermediate adsorbed in an η^2 configuration, the equilibrium arrows (⇄) with a circle indicate that an elementary step is quasi-equilibrated, and k_x is the rate constant for elementary step x.

near saturation coverages[55,56] and facile decomposition of H_2O_2 on Pd surfaces,[5,12] which suggest that these species readily desorb and adsorb at rates greater than measured turnover rates (1×10^{-3}−7×10^{-1} $(Pd_s \cdot s)^{-1}$). Subsequently, O_2** undergoes either quasi-equilibrated proton−electron transfer (Scheme 1, step 4) to form hydroperoxy (OOH**) or irreversibly cleaves the O−O bond (Scheme 1, step 7) to form chemisorbed oxygen atoms (O*). Adsorbed OOH** then reacts by kinetically relevant proton−electron transfer (Scheme 1, step 5) to form H_2O_2** or dissociates by irreversible O−O rupture (Scheme 1, step 8). Finally, H_2O_2** desorbs to the liquid-phase (Scheme 1, step 6) or dissociates (Scheme 1, step 12) to form two hydroxyls (OH*). Following irreversible O−O bond rupture in O_2** (Scheme 1, step 7), OOH** (Scheme 1, step 8), or H_2O_2** (Scheme 1, step 12), O* and OH* species hydrogenate (Scheme 1, steps 9 and 10) to form H_2O*, which then desorbs (Scheme 1, step 11).

Scheme 1 suggests net H_2O_2 formation rates ($r_{H_2O_2}$) that increase with the number of hydroperoxy surface intermediates ([OOH**]) and with the concentration of H^+ in solution and decrease with the number of adsorbed H_2O_2 molecules ([H_2O_2**]).

$$r_{H_2O_2} = k_5[OOH**][H^+][e^-] - k_{12}[H_2O_2**] \quad (2)$$

where k_5 is the rate constant for proton−electron transfer to OOH**, $[H^+]$ is the concentration of H^+ in the solvent, $[e^-]$ is the number of free e^- on the cluster (provided by heterolytic

DOI: 10.1021/jacs.5b10669
J. Am. Chem. Soc. 2016, 138, 574−586

oxidation of H_2; Scheme 1, steps 1 and 2), and k_{12} is the rate constant for O−O rupture within H_2O_2**. Applying the pseudo-steady-state hypothesis (PSSH) to [OOH**] and other reactive intermediates involved in H_2O_2 formation and decomposition gives the rate equation

$$r_{H_2O_2} = \left(k_5K_4K_3K_2^2K_1(O_2)(H_2) - \frac{k_{12}}{K_6}(H_2O_2)\right)[**] \quad (3)$$

in which k_x and K_x are rate and equilibrium constants respectively for each step x, (H_2O_2) is the liquid-phase concentration of H_2O_2, and [**] is the number of unoccupied sites available to bind species containing dioxygen (i.e., −O−O−) in η^2 configurations.[57−59] An expression for [**] is given from first summing the numbers of likely surface intermediates

$$[L] = [**] + [O_2**] + [OOH**] + [H_2O_2**] \quad (4)$$

where $[L]$ and $[O_2**]$ are the number of available surface sites and O_2** intermediates, respectively. Formation rates of H_2O_2 and H_2O do not depend on (O_2) over the pressure range tested (Figure 2), indicating that the MARI contains oxygen and thus that H* coverages are insignificant. Moreover, coverages of dissociation products (i.e., O*, OH*) appear to be low on active sites because H_2O_2 and H_2O rate expressions derived after assuming a MARI of either O* or OH* (Supporting Information section S6) were inconsistent with measured rate dependencies on H_2 and O_2 pressures (Figure 2). Equation 4 can be re-expressed in terms of the rate and equilibrium constants as well as reactant pressures and concentrations:

$$[L] = [**] + K_3(O_2)[**] + K_4K_3K_2K_1^{1/2}(H_2)^{1/2}(O_2)[**] + \frac{1}{K_6}(H_2O_2)[**] \quad (5)$$

The combination of eqs 3 and 5 yields the rate expression for H_2O_2 formation:

$$\frac{r_{H_2O_2}}{[L]} = \frac{k_5K_4K_3K_2^2K_1(H_2)(O_2) - \frac{k_{12}}{K_6}(H_2O_2)}{1 + K_3(O_2) + K_4K_3K_2K_1^{1/2}(H_2)^{1/2}(O_2) + \frac{1}{K_6}(H_2O_2)} \quad (6)$$

The complete derivation of this rate expression and alternative rate expression that utilize other assumptions (and do not match the experimental data) are provided in Supporting Information section S6. H_2O_2 selectivities do not change significantly with H_2 conversion (or residence time) under the conditions used here (<10% H_2 conversion, Figure S2.3), which shows that the rate of H_2O_2 decomposition (Scheme 1, step 12, $(k_{12}/k_6)(H_2O_2)$) is negligible compared to the rate of H_2O_2 formation (Scheme 1, step 5). Thus, H_2O_2 decomposition can be neglected, and the forward rate for H_2O_2 formation (r_5) is equal to the net rate ($r_{H_2O_2}$). Active sites become saturated with molecular oxygen (i.e., O_2** is the MARI) in the limit of low (H_2), and the rate equation simplifies to

$$\frac{r_{H_2O_2}}{[L]} = k_5K_4K_2^2K_1(H_2) \quad (7)$$

Equation 7 is consistent with H_2O_2 formation rates that increase in proportion to (H_2) at the lowest values of (H_2) (Figure 2a, 5−150 kPa H_2), and which do not depend on (O_2) (Figure 2a, 25−400 kPa). The coverage of OOH** increases with (H_2) such that OOH** becomes the MARI when (H_2) is greater than 150 kPa, which causes eq 6 to take the form

$$\frac{r_{H_2O_2}}{[L]} = k_5K_2K_1^{1/2}(H_2)^{1/2} \quad (8)$$

This expression agrees with H_2O_2 formation rates that remain independent of (O_2) and which increase as $(H_2)^{1/2}$ in the range of 200−400 kPa H_2 (Figure 2a). The mechanism described for H_2O_2 formation proposed in Scheme 1 and the derived rate expression (eq 6) are therefore consistent with measured H_2O_2 formation rates over the full range of conditions tested.

Scheme 1 shows that the rate of H_2O formation (r_{H_2O}) equals the summed rates of irreversible O−O bond scission[12] within all dioxygen-containing surface species (i.e., O_2**, OOH**, and H_2O_2**) at steady-state. The rate of O−O bond scission in these three species is given by

$$r_{H_2O} = k_7[O_2**] + k_8[OOH**] + k_{12}[H_2O_2**] \quad (9)$$

which takes a new form after accounting for the quasi-equilibrated steps in Scheme 1

$$r_{H_2O} = \left(k_7K_3(O_2) + k_8K_4K_3K_2K_1^{1/2}(H_2)^{1/2}(O_2) + \frac{k_{12}}{K_6}(H_2O_2)\right)[**] \quad (10)$$

Implementing the site balance yields the rate equation for H_2O formation:

$$\frac{r_{H_2O}}{[L]} = \frac{k_7K_3(O_2) + k_8K_4K_3K_2K_1^{1/2}(H_2)^{1/2}(O_2) + \frac{k_{12}}{K_6}(H_2O_2)}{1 + K_3(O_2) + K_4K_3K_2K_1^{1/2}(H_2)^{1/2}(O_2) + \frac{1}{K_6}(H_2O_2)} \quad (11)$$

The rate of H_2O formation by H_2O_2 decomposition (Scheme 1, step 12; $(k_{12}/k_6)(H_2O_2)$) is negligible in comparison to H_2O formation by O_2** and OOH** decomposition, as already discussed. Density functional theory calculations show that O−O bond dissociation barriers are ≥40 kJ mol^{-1} lower in OOH** than for O_2** on Pd surfaces,[10,11,44] which agrees qualitatively with homolytic bond dissociation energies (BDE) that are 230 kJ mol^{-1} greater for the O−O bond in O_2(g) than for that in ·OOH(g) radicals.[60] Together these results imply that rate constants and likely rates for OOH** dissociation may be much higher than those for O_2** on Pd clusters. The combination of these assumptions yields the following simplified rate expression

$$\frac{r_{H_2O}}{[L]} = \frac{k_8K_4K_3K_2K_1^{1/2}(H_2)^{1/2}(O_2)}{1 + K_3(O_2) + K_4K_3K_2K_1^{1/2}(H_2)^{1/2}(O_2) + \frac{1}{K_6}(H_2O_2)} \quad (12)$$

At low (H_2) (<150 kPa H_2), O_2** is the MARI, and eq 12 becomes

$$\frac{r_{H_2O}}{[L]} = k_8K_4K_2K_1^{1/2}(H_2)^{1/2} \quad (13)$$

and as seen for H_2O_2 formation rates, OOH** is the MARI at higher (H_2) (200−400 kPa H_2), giving

$$\frac{r_{H_2O}}{[L]} = k_8 \quad (14)$$

These simplified rate expressions (i.e., eqs 13 and 14) are consistent with H_2O formation rates that are constant for all (O_2) and that transition from a half- to zero-order dependence on (H_2) at ∼150 kPa (Figure 2b). These comparisons show that O−

DOI: 10.1021/jacs.5b10669
J. Am. Chem. Soc. 2016, 138, 574−586

O bond rupture occurs primarily within OOH** surface intermediates, which agrees also with mechanistic predictions for the ORR reaction on Pt surfaces.[61,62]

The rate equations for H_2O_2 (eq 6) and H_2O (eq 12) formation suggest that the selectivity towards H_2O_2 will increase with (H_2) while remaining constant for all (O_2) values. These expectations are shown clearly when H_2O_2 selectivity is expressed as the ratio of H_2O_2 and H_2O formation rates (χ):

$$\chi = \frac{r_{H_2O_2}}{r_{H_2O}} = \frac{k_5 K_2 K_1^{1/2} (H_2)^{1/2}}{k_8} \quad (15)$$

The value of χ does not depend on the identity of the MARI, because pathways for H_2O_2 and H_2O formation occur on the same active sites. Figure 3 shows that χ values increase as $(H_2)^{1/2}$

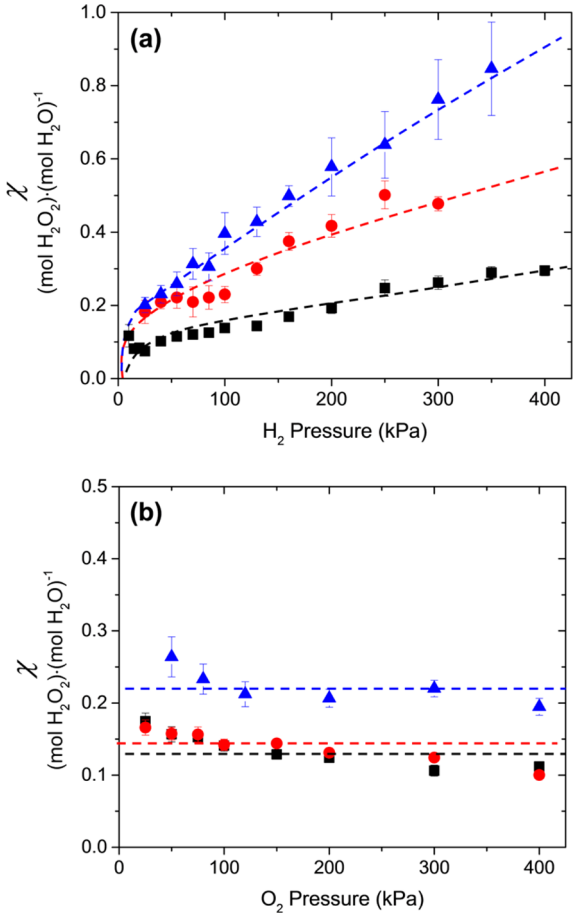

Figure 3. Ratio of the formation of H_2O_2 to that for H_2O (χ) as a function of (a) H_2 pressure at 60 kPa O_2 and (b) O_2 pressure at 60 kPa H_2 on 0.7 nm (black ■), 3 nm (red ●), and 7 nm (blue ▲) Pd clusters (277 K, 10 cm^3 min^{-1} CH_3OH). Lines are intended to guide the eye.

(Figure 3a) and remain constant with changing (O_2) (Figure 3b) on 0.7 nm Pd clusters. These comparisons show that the expression for χ is consistent with the rate data (Figure 2). The interpretation of these results shows that O−O bonds cleave at negligible rates in O_2** and H_2O_2** intermediates and that both H_2O_2 and H_2O form on the same sites. The values of χ increase by a factor of 2 on 0.7 nm Pd clusters as (H_2) increases over the range 5−400 kPa (Figure 3a) and demonstrate that significant increases in selectivity can be achieved by increasing (H_2). These findings (Figure 3) differ from previous studies that reported H_2O_2 selectivities that decreased with increasing H_2/O_2 reactant ratios;[21,63,64] however, those studies did not discuss precautions taken to measure primary formation rates for H_2O_2 and H_2O and may include contributions from H_2O_2** decomposition, which would complicate analysis.

In contrast to the previously proposed Langmuir−Hinshelwood mechanisms,[10,11,47] the findings of this work implicate a proton−electron transfer mechanism (Scheme 1, steps 4 and 5) as the primary pathway for H_2O_2 formation. Notably, this mechanism resembles proposals for the two-electron ORR to H_2O_2,[46,65] however, without an applied electrical potential. Instead, the catalytic direct synthesis of H_2O_2 on silica-supported Pd clusters is driven by the chemical potential of the supplied H_2(g). This mechanism requires that each Pd cluster catalyzes both electrochemical half-reactions in order to conserve charge (Scheme 2). To further confirm the role of proton and electron

Scheme 2. Pd Clusters Catalyze Both Heterolytic H_2 Oxidation and O_2 Reduction Steps in Order to Form H_2O_2 at Steady-State while Conserving Charge

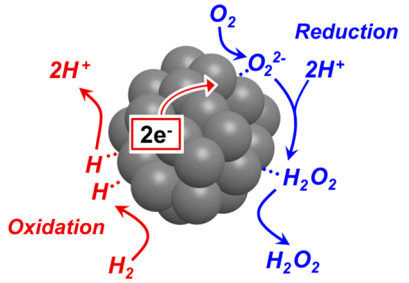

transfer pathways in the direct synthesis of H_2O_2, we next describe how H_2O_2 formation rates require that H^+ are present in the solvent.

3.2. Effects of H^+ Concentration on H_2O_2 and H_2O Formation Rates. The proposed mechanism for H_2O_2 formation (Schemes 1 and 2) contains steps identical to charge-transfer processes for the ORR.[46,65] These steps are well-accepted when an electrical potential is applied between two metal electrodes separated by an electrolyte; however, they are not commonly invoked to describe reactions at the surface of nanoclusters supported on insulators (e.g., Pd−SiO_2). Figure 4 shows that increases in the H_2O_2 concentration over time within a semibatch reactor are much greater in protic solvents (e.g., methanol and water) than in aprotic solvents (e.g., acetonitrile, dimethyl sulfoxide, and propylene carbonate) (4.2 kPa H_2, 4.2 kPa O_2, 295 K, 3.8 wt % Pd−SiO_2). Primary formation rates for H_2O_2 are calculated from the change in H_2O_2 concentration with time at the early stages of each experiment (0−0.17 h), and the results are shown in Table 2 along with the pK_a values and dielectric constant for each solvent. These data (Figure 4 and Table 2) show that the H_2O_2 turnover rates in protic solvents are at least 10^3 times greater than those in aprotic solvents (whose H_2O_2 turnover rates fall below the detection limit of the experiment, $<1.7 \times 10^{-6}$ (mol H_2O_2) (mol Pd_s s)$^{-1}$). Turnover rates depend on the protic−aprotic nature of the solvent but do not correlate with the dielectric constants of the solvents (Table 2), which suggests that H_2O_2 formation is not sensitive to solvent polarity. These data (Table 2) are completely consistent with our proposed mechanism (Schemes 1 and 2); moreover, these results cannot be explained by mechanisms for direct synthesis that only involve elementary steps describing reactions between coadsorbed surface intermediates (e.g., O_2* + H* → OOH* + *), which are not influenced by H^+. We next discuss rate

DOI: 10.1021/jacs.5b10669
J. Am. Chem. Soc. 2016, 138, 574−586

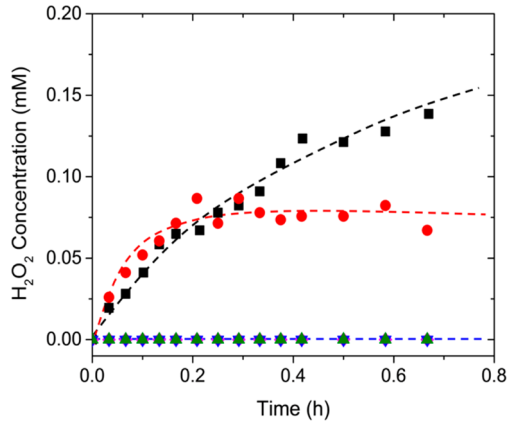

Figure 4. H_2O_2 concentrations as functions of time during direct synthesis in a well-mixed semibatch reactor using protic (methanol (black ■) and water (red ●)) or aprotic (dimethyl sulfoxide (green ▲), acetonitrile (blue ▼), and propylene carbonate (magenta ♦)) solvents (4.2 kPa H_2, 4.2 kPa O_2, 40 cm^3 solvent, 20 mg of 3.8 wt % Pd−SiO_2, 295 K). Lines are intended to guide the eye.

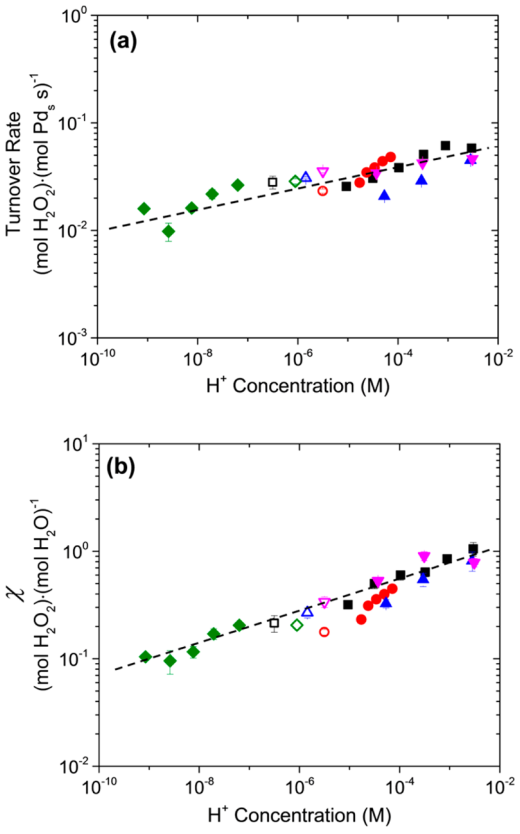

Figure 5. (a) H_2O_2 turnover rates and (b) ratio of the formation of H_2O_2 to that for H_2O (χ) on 0.7 nm Pd clusters as a function of H^+ concentration, which was controlled by the addition of a mineral acid or base including H_2SO_4 (black ■), H_3PO_4 (blue ▲), HCl (magenta ▼), $NaHCO_3$ (green ♦), or H_2CO_3 (red ●, by applying 0−0.7 MPa CO_2) (50 kPa H_2, 60 kPa O_2, 277 K, 10 cm^3 min^{-1} 20% v/v CH_3OH). Empty symbols represent measurements taken prior to the addition of each acid or base. Lines are intended to guide the eye.

measurements conducted as a function of H^+ concentration using multiple H^+ donors and acceptors and interpret these data using the previously derived rate expressions (eqs 6 and 12) to clarify the role of mineral acids commonly used to increase H_2O_2 selectivities during direct synthesis.[21,22]

Figure 5 shows that steady-state H_2O_2 formation rates (Figure 5a) and χ (Figure 5b) depend weakly on the H^+ concentration,[66] which is changed by adding H_2SO_4, H_3PO_4, HCl, $NaHCO_3$, or H_2CO_3 (via dissolved CO_2) to the solvent (50 kPa H_2, 60 kPa O_2, 20% v CH_3OH, 277 K). Figure 5a demonstrates that formation rates for H_2O_2 increase with increasing H^+ concentration ($r_{H_2O_2} \sim [H^+]^{0.1}$) and are similar at any given H^+ concentration. These data are qualitatively consistent with our proposed mechanism for H_2O_2 formation (Scheme 1), which is shown by restating the simplified rate expressions for H_2O_2 formation (eqs 7 and 8) in terms of the H^+ concentration. The quasi-equilibrated steps for heterolytic H_2 oxidation (Scheme 1, steps 1 and 2) show that the H_2 pressure and the concentrations of H^+ and free e^- are related by

$$[H^+]^2[e^-]^2 = K_2^2K_1(H_2) = \alpha \tag{16}$$

where $[H^+]$ and $[e^-]$ are the proton and electron concentrations, respectively, and α is a constant equal to the product of the equilibrium constants ($K_2^2K_1$) and the H_2 pressure under the conditions of these experiments (Figure 5). Substitution of eq 16 into the rate equations for H_2O_2 formation yields a second-order dependence on both $[H^+]$ and $[e^-]$ when O_2** is the MARI:

$$\frac{r_{H_2O_2}}{[L]} = (k_5K_4)[H^+]^2[e^-]^2 \tag{17}$$

and a first-order dependence on $[H^+]$ and $[e^-]$ when OOH** is the MARI:

$$\frac{r_{H_2O_2}}{[L]} = (k_5K_2K_1^{1/2})[H^+][e^-] \tag{18}$$

H_2O_2 formation rates are undetectable in the absence of an e^- source (i.e., 0 kPa H_2, Figure 2), even in solutions with a high $[H^+]$ (pH 3, 0.5 mM H_2SO_4 in H_2O), which is in agreement with eqs 17 and 18 and previous measurements.[21] The addition of proton donors (i.e., mineral acids) to the solvent gives a

Table 2. Initial Rates of H_2O_2 Formation in Protic and Aprotic Solvents with Different Dielectric Constants[a]

solvent	protic/aprotic	pK_a	dielectric constant (ε)	H_2O_2 formation rate ((mol H_2O_2) (mol Pd_s s)$^{-1}$)
methanol	protic	16	32.6	1.5×10^{-3}
water	protic	16	78.5	1.3×10^{-3}
dimethyl sulfoxide	aprotic	35	47.0	$<1.7 \times 10^{-6}$
acetonitrile	aprotic	25	37.5	$<1.7 \times 10^{-6}$
propylene carbonate	aprotic	40−50[b]	64.0	$<1.7 \times 10^{-6}$

[a]Initial rates of H_2O_2 formation were calculated by a linear fit of measured H_2O_2 concentrations within a semibatch reactor over the range of 0−0.17 h. Data was collected on the 3.8 wt % Pd−SiO_2 catalyst at 4.2 kPa H_2 and 4.2 kPa O_2. [b]Estimated from standard pK_a values for alkyl groups as well as induction effects from oxygen atoms within the molecule[72]

DOI: 10.1021/jacs.5b10669
J. Am. Chem. Soc. 2016, 138, 574−586

measurable increase in $[H^+]$ due to the dissociation of these species:

$$[HX] \overset{K_{HX}}{\longleftrightarrow} [H^+] + [X^-] \quad (19)$$

where K_{HX} is the equilibrium constant for acid dissociation and $[HX]$ and $[X^-]$ are the concentrations of mineral acids and counterions in the solution, respectively. H_2O_2 formation rates increase only slightly when proton donors are added to the solvent ($r_{H_2O_2} \sim [H^+]^{0.1}$, Figure 5a) because $[H^+]$ and $[e^-]$ are inversely proportional to one another as dictated by the equilibrium for heterolytic H_2 oxidation (eq 16). Thus, the addition of acid increases $[H^+]$ by a certain factor but simultaneously decreases $[e^-]$ by the same amount. Consequently, we attribute the small increase in H_2O_2 formation rates to electronic modification of the solution at the liquid−solid interface induced by the presence of counterions (i.e., Cl^-, SO_4^{2-}, HCO_3^-, and $H_2PO_4^-$), which increase with the amount of acid added to the solvent. The H_2O turnover rates show also a weak inverse dependence on $[H^+]$ ($r_{H_2O} \sim [H^+]^{-0.05}$; Figure S7.1). The H_2O formation rate does not directly depend on $[H^+]$; therefore, these small changes should only reflect the adsorption of counterions onto the Pd, which are likely present at low coverages.[67−69] These results agree with previous observations that strongly binding anions decrease H_2O formation rates during ORR, perhaps because the anions must be displaced from the surface prior to O−O bond rupture.[49−51] Additional measurements that probe counterion surface coverages, perhaps by in situ infrared spectroscopy, are needed in order to develop a deeper understanding of the manner by which rates and selectivities are influenced specifically by counterions. Overall, the addition of proton donors increases the selectivity toward H_2O_2 (i.e., χ, Figure 5b) by both increasing H_2O_2 formation rates (Figure 5a) and decreasing H_2O formation rates (Figure S7.1). These observed trends are similar among all mineral acids tested; therefore, χ can be increased significantly (10-fold) by adding acids to the system (10^{-9}−10^{-2} M H^+) with little dependence on the identity of the counterion.

Collectively, these data (Figures 4 and 5) show that both H^+ and e^- are required to produce H_2O_2, which helps to clarify the previously vague role of acids for H_2O_2 formation.[21,24] These results and their interpretation are consistent with the proposed mechanism for H_2O_2 formation (Schemes 1 and 2). Moreover, our measurements cannot be explained by Langmuirian mechanisms that involve homolytic hydrogenation steps, occurring at one or even two distinct surface sites. These results also explain the reported benefits of using CO_2 as a diluent during direct synthesis of H_2O_2.[16,70,71] H_2CO_3, formed following dissolution of CO_2 in protic solvents, provides HCO_3^- and CO_3^{2-} counterions that may bind to Pd clusters or alter the properties of the solution near the surface of these clusters, and increase H_2O_2 selectivities, as shown above. Thus, high-pressure CO_2 can replace strong mineral acids (e.g., H_2SO_4 and HCl) that are less environmentally benign. However, to be competitive with AO, direct synthesis will require higher selectivities than those achieved here on 0.7 nm Pd−SiO_2 from the addition of CO_2 alone (31% H_2O_2 selectivity). In the next section, we show that higher H_2O_2 selectivities are achieved when we decrease the extent of e^- back-donation to adsorbed oxygen species by increasing the size of the Pd clusters.

3.3. Effects of Pd Cluster Size on Selectivities and Activation Enthalpies. Changes in the size of Pd clusters lead to changes in both H_2O_2 selectivities and turnover rates that reflect significant differences between the electronic structures of Pd clusters caused, in turn, by changes to the degree of coordinative saturation of surface atoms. Figure 3 shows that values of χ increase monotonically with the size of Pd clusters at all H_2 or O_2 pressures, and 7 nm Pd gives χ values that are more than three times greater than those for 0.7 nm Pd under all conditions, which agrees qualitatively with comparisons between H_2O_2 selectivities for 3.4 and 4.2 nm Pd clusters on SiO_2.[27] In addition, H_2O_2 turnover rates are much larger on 7 nm Pd clusters than those on 0.7 nm Pd (Figures S9.2a and 2a, respectively). The rate ratios for all Pd clusters (Figure 3) increase with a half-order dependence on (H_2) and do not depend on (O_2) (Figure S8.1 shows linearized rates). The change in H_2O_2 and H_2O formation rates with changes in (H_2) and (O_2) on 3 and 7 nm clusters (Figures S9.1 and S9.2) are described accurately by the mechanism (Scheme 1) and rate equations (eqs 6 and 12) given earlier. These differences in turnover rates and selectivities between Pd clusters of different sizes result, therefore, from changes in the stability of surface intermediates and transition states and not from differences between the mechanisms for H_2O_2 and H_2O formation on clusters of different sizes. The changes in the stability of reactive intermediates are reflected in the values of the apparent activation enthalpies ($\Delta H^{\ddagger}$) and entropies ($\Delta S^{\ddagger}$) for these reactions, determined from measurements of rates as a function of temperature.

Transition state theory proposes that reactant species (e.g., OOH* and a H^+−e^- pair) exist in equilibrium with the transition state (H^+−OOH**‡) for a given elementary step.[72] Close agreement between measured H_2O_2 and H_2O formation rates (Figures 2, S9.1, and S9.2) and rate expressions (eqs 6 and 12) suggest that these reactant species also exist in quasi-equilibrium with gaseous H_2 and O_2 reactants. These multiple equilibrated steps and the form of eq 7, therefore, suggest that the transition states for H_2O_2 formation are equilibrated also with chemisorbed oxygen (O_2**) and H_2, as shown in Scheme 3 and expressed in the following reaction:

$$O_2{**} + H_2(g) \overset{K^{\ddagger}_{H_2O_2}}{\longleftrightarrow} H^+ - OOH{**}^{\ddagger} \quad (20)$$

where $K^{\ddagger}_{H_2O_2}$ is the transition state equilibrium constant for H_2O_2 formation. By using conventions of transition state theory, the rate of H_2O_2 formation can be expressed in terms of the number of transition state species ($[H^+$−OOH**$^{\ddagger}]$):

$$\frac{r_{H_2O_2}}{[L]} = \frac{k_B T}{h}[H^+\text{−}OOH{**}^{\ddagger}] \quad (21)$$

where T is the temperature in Kelvin, and h and k_B are Planck's and Boltzmann's constants, respectively. The equilibrated nature of eq 20, along with the observation that H_2O_2 formation is independent of (O_2) (Figure 2a) allow eq 21 to be re-expressed in terms of (H_2) and $K^{\ddagger}_{H_2O_2}$:

$$\frac{r_{H_2O_2}}{[L]} = \frac{k_B T}{h} K^{\ddagger}_{H_2O_2}(H_2) \quad (22)$$

Supporting Information section 10 contains equivalent expressions for H_2O formation. Figure 6 shows calculated values for $K^{\ddagger}_{H_2O_2}$ and $K^{\ddagger}_{H_2O}$ (eqs 22 and S10.3) as a function of inverse temperature, and these values reflect only primary formation rates, calculated at zero H_2 conversion by extrapolating rates measured as a function of residence time at every temperature (Figure S2.2).

DOI: 10.1021/jacs.5b10669
J. Am. Chem. Soc. 2016, 138, 574−586

Scheme 3. Thermochemical Cycle Showing the Changes in Free Energy at Each Step for the Direct Synthesis of H_2O_2 (Blue) and H_2O (Red) on Pd Clusters[a]

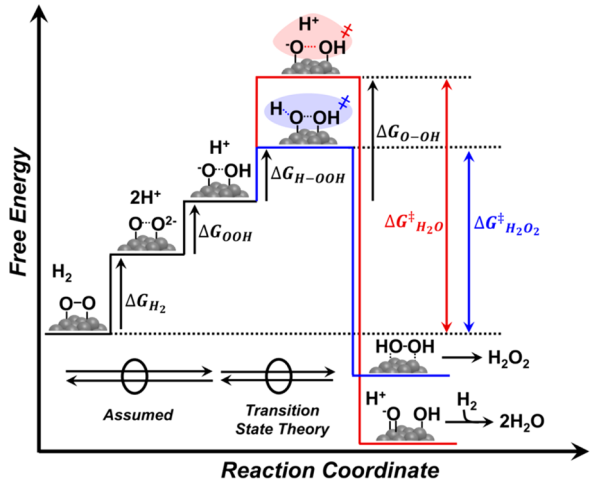

[a]Changes in free energy are shown for the heterolytic dissociation of H_2 (ΔG_{H_2}) and the protonation of O_2** (ΔG_{OOH}) and OOH** (ΔG_{H-OOH}). The sum of these free energy differences corresponds to the measured activation free energy for H_2O_2 formation on O_2-saturated Pd clusters ($\Delta G^{\ddagger}_{H_2O_2}$). The measured activation free energy for H_2O formation ($\Delta G^{\ddagger}_{H_2O}$) corresponds to the sum of ΔG_{H_2}, ΔG_{OOH}, and the change in free energy for O−O bond scission in OOH** (ΔG_{O-OH}).

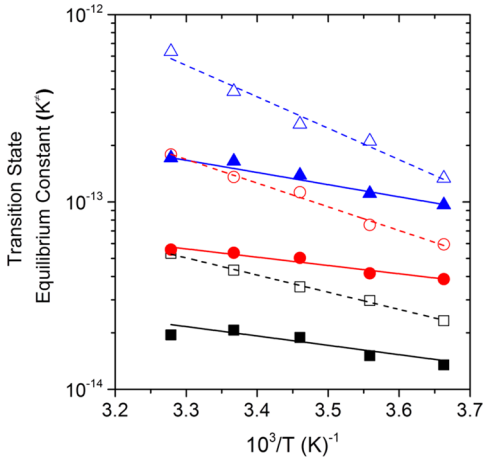

Figure 6. Transition state equilibrium constants $K^{\ddagger}$ for H_2O_2 (solid symbols) and H_2O (empty symbols) formation as a function of inverse temperature on 0.7 nm Pd (black ■ and □), 3 nm Pd (red ● and ○), and 7 nm Pd (blue ▲ and Δ) clusters (50 kPa H_2, 60 kPa O_2, 20% v/v CH_3OH). Turnover rates used to calculate $K^{\ddagger}$ values were determined at zero H_2 conversion by extrapolating turnover rates measured at three different conversions, each less than 10%. Lines represent fits to the Eyring equation.

Values of $\Delta H^{\ddagger}$ and $\Delta S^{\ddagger}$ are determined from the temperature dependence of the overall change in free energy for H_2O_2 ($\Delta G^{\ddagger}_{H_2O_2}$) and H_2O ($\Delta G^{\ddagger}_{H_2O}$) formation (Scheme 3). $\Delta G^{\ddagger}_{H_2O_2}$ equals the sum of energies for the dissociation of H_2(g) to H^+ and to e^- localized on adsorbed O_2** (ΔG_{H_2}), protonation of O_2^{2-}** to hydroperoxy (ΔG_{OOH}), and protonation of OOH^-** to form the transition state (ΔG_{H-OOH}):

$$\Delta G^{\ddagger}_{H_2O_2} = \Delta G_{H_2} + \Delta G_{OOH} + \Delta G_{H-OOH} \quad (23)$$

whereas $\Delta G^{\ddagger}_{H_2O}$ includes the free energy change for activating the O−O bond in OOH** (ΔG_{O-OH}):

$$\Delta G^{\ddagger}_{H_2O} = \Delta G_{H_2} + \Delta G_{OOH} + \Delta G_{O-OH} \quad (24)$$

Lastly, transition state theory allows values of $K^{\ddagger}_x$ (Figure 6) to be expressed in terms of $\Delta G^{\ddagger}$ as well as $\Delta H^{\ddagger}$ and $\Delta S^{\ddagger}$ (from $\Delta G^{\ddagger} = \Delta H^{\ddagger} - T\Delta S^{\ddagger}$):

$$K^{\ddagger}_x = e^{-\Delta G^{\ddagger}_x/RT} = e^{-\Delta H^{\ddagger}_x/RT} e^{\Delta S^{\ddagger}_x/R} \quad (25)$$

where R is the ideal gas constant and the subscript x indicates that the associated variable corresponds to the formation of product x.

Table 3 shows values of $\Delta H^{\ddagger}_{H_2O_2}$ and $\Delta H^{\ddagger}_{H_2O}$ for 0.7, 3, and 7 nm Pd clusters calculated from $K^{\ddagger}_{H_2O_2}$ and $K^{\ddagger}_{H_2O}$ (Figure 6 and eq 25). $\Delta H^{\ddagger}_{H_2O_2}$ values increase from 9 to 14 ± 2 kJ mol^{-1} as the mean sizes of Pd clusters increase, which shows that $\Delta H^{\ddagger}_{H_2O_2}$ is weakly sensitive to cluster size. These $\Delta H^{\ddagger}_{H_2O_2}$ values are similar to barriers for proton−electron transfer steps on Pt electrocatalysts determined from DFT calculations (~10 kJ mol^{-1})[73,74] and measured experimentally (<15 kJ mol^{-1})[75] as well as estimates (10−20 kJ mol^{-1}) for other ORR electrocatalysts.[75−77] Such comparisons indicate that these charge-transfer processes depend weakly on the coordinative saturation and the elemental identity of group 8 metal surfaces. The strong agreement between this work and these previous studies[73−77] provides further evidence that the mechanisms for direct synthesis of H_2O_2 are comparable to those for the electrochemical ORR. Measured $\Delta H^{\ddagger}_{H_2O_2}$ values are significantly lower than calculated barriers for hydrogenation of molecular oxygen (77−109 kJ mol^{-1}) on Pd,[10,11] which shows that direct synthesis of H_2O_2 should proceed predominantly by proton−electron transfer and not by hydrogenation. Measured values for $\Delta H^{\ddagger}_{H_2O}$, in contrast, increase from 18 to 32 ± 2 kJ mol^{-1} as the mean diameters of Pd clusters increase from 0.7 to 7 nm (Table 3), and $\Delta H^{\ddagger}_{H2O}$ clearly depends on the coordinative saturation of the exposed Pd atoms. Notably, $\Delta H^{\ddagger}_{H_2O}$ on 7 nm Pd clusters, whose surfaces primarily expose close-packed terraces,[78] match activation energies (~30 kJ mol^{-1}) for O−O bond dissociation within chemisorbed O_2 on

Table 3. Catalyst Activation Enthalpies and Entropies for H_2O_2 and H_2O Formation[a]

sample	$\Delta H^{\ddagger}_{H_2O_2}$ (kJ mol^{-1})	$\Delta H^{\ddagger}_{H_2O}$ (kJ mol^{-1})	$\Delta S^{\ddagger}_{H_2O_2}$ (J mol^{-1} K^{-1})	$\Delta S^{\ddagger}_{H_2O}$ (J mol^{-1} K^{-1})
0.7 nm Pd−SiO_2	9 ± 2	18 ± 2	−232 ± 23	−197 ± 20
3 nm Pd−SiO_2	9 ± 2	24 ± 2	−226 ± 23	−165 ± 17
7 nm Pd−SiO_2	14 ± 2	32 ± 3	−200 ± 20	−129 ± 13

[a]Activation enthalpies and entropies were calculated from measured transition state equilibrium constants ($K^{\ddagger}$) and eq 25. Error was estimated to be 10% of the measured value based on the maximum error recorded for the turnover rate measurements used to calculate $\Delta H^{\ddagger}$ and $\Delta S^{\ddagger}$.

DOI: 10.1021/jacs.5b10669
J. Am. Chem. Soc. 2016, 138, 574−586

Pd(111).[79,80] This quantitative agreement supports our conclusion that H_2O forms following kinetically relevant O−O bond scission on Pd. The smallest Pd clusters (0.7 nm) give the lowest $\Delta H^{\ddagger}_{H_2O}$ values (18 kJ mol^{-1}) because these clusters expose a greater fraction of undercoordinated surface sites[78] that possess a greater density of states near the Fermi level as a result of less overlap between the d orbitals of Pd atoms.[32] O−O bond dissociation barriers that decrease with the decreasing coordinative saturation of surface Pd atoms (Table 3) agree with published comparisons for O_2 dissociation on Pd(111),[79,80] Pd(100),[81,82] and Pd(110)[83] surfaces. Thus, the amount of charge back-donated to $2\pi^*$ of O_2 on 0.7 nm clusters is greater than that for 7 nm Pd clusters, which is reflected in the $\Delta H^{\ddagger}_{H_2O}$ values. Consequently, H_2O_2 selectivities (i.e., χ values) increase with the size of the Pd clusters because O−O bond rupture transition states are more sensitive to electronic changes in the Pd surface than those for proton−electron transfer (Figure 3).

Table 3 shows values for $\Delta S^{\ddagger}_{H_2O_2}$ and $\Delta S^{\ddagger}_{H_2O}$ on Pd clusters. These $\Delta S^{\ddagger}$ values are large and negative, which shows that the formation of the transition states for each pathway involve a significant loss of entropy. Here, $\Delta S^{\ddagger}_{H_2O_2}$ corresponds to the difference in entropy of the product and reactant states of the process depicted in Scheme 3 such that

$$\Delta S^{\ddagger}_{H_2O_2} = S_{H_2O_2^{\ddagger}} - S_{H_2} - S_{O_2**} \quad (26)$$

and a corresponding equation describes $\Delta S^{\ddagger}_{H_2O}$:

$$\Delta S^{\ddagger}_{H_2O} = S_{H_2O^{\ddagger}} - \frac{1}{2}S_{H_2} - S_{O_2**} \quad (27)$$

where $S_{H_2O_2^{\ddagger}}$ and $S_{H_2O^{\ddagger}}$ are the entropies of the transition states for H_2O_2 and H_2O formation, respectively, whereas S_{H_2} and S_{O_2**} are the entropies of H_2 and O_{2**}. Values of $\Delta S^{\ddagger}_{H_2O_2}$ (−232 to −200 J mol^{-1} K^{-1}) and $\Delta S^{\ddagger}_{H_2O}$ (−197 to −129 J mol^{-1} K^{-1}) are shown in Table 3.

For H_2O_2 formation, the difference between the entropies of the reactants (O_2** and H_2(g)) and that of the transition state (H^+−OOH**‡) can be estimated roughly as being equal to the translational and rotational entropy loss from binding H_2(g) to O_2** (i.e., S_{H_2}, 131 J mol^{-1} K^{-1} at 101 kPa H_2, 273 K[84]). The values of $\Delta S^{\ddagger}_{H_2O_2}$ (Table 3), however, are much more negative (by >70 J mol^{-1} K^{-1}) than the estimate from this simple approximation. These significant differences suggest that additional entropy is lost, perhaps, as the hydrogen-bonded solvent reorganizes into a lower energy configuration about the hydrophilic transition state,[85] which forms at the interface between water and the hydrophobic O_2**-covered metal cluster.[86] Such a process would also be consistent with values of $\Delta S^{\ddagger}_{H_2O}$ that also reflect a much larger entropy loss (again by >70 J mol^{-1} K^{-1}) than estimated by the consumption of one-half of a H_2(g) molecule. Estimates for the exact entropic change caused by reorganization of the solvating molecules falls beyond the scope of this study. Values of both $\Delta S^{\ddagger}_{H_2O_2}$ and $\Delta S^{\ddagger}_{H_2O}$ become slightly more positive (i.e., less entropy is lost) as the size of Pd clusters increase (Table 3). These changes show that entropies of the transition states (i.e., $S_{H_2O_2^{\ddagger}}$ and $S_{H_2O^{\ddagger}}$) increase more with the size of Pd clusters than the surface intermediate from which they form (i.e., S_{O_2**}) because S_{H_2} does not depend on the size of Pd clusters. This comparison implies that the transition states gain more translational mobility than does O_2** as the coordinative saturation of the Pd surface atoms increases.

These data and the interpretations presented here show that increasing the coordination of Pd atoms at cluster surfaces increases the H_2O_2 selectivity (χ) by increasing $\Delta H^{\ddagger}_{H_2O}$ while only slightly affecting $\Delta H^{\ddagger}_{H_2O_2}$ values. The weak dependence of $\Delta H^{\ddagger}_{H_2O_2}$ on the electronic structure of the surface is consistent with the proposed mechanism for H_2O_2 formation (Schemes 1 and 2) because H_2O_2 forms by proton−electron transfer that involves liquid-phase reactants insensitive to the electronic structure of the catalyst surface. In contrast, $\Delta H^{\ddagger}_{H_2O}$ depends on the coordination of Pd surface atoms because the propensity of surfaces to cleave O−O bonds depends strongly on their electronic structure. The increase in $\Delta S^{\ddagger}$ values with cluster size shows that the transition states for H_2O_2 and H_2O formation both become more mobile relative to O_2** as the size of Pd clusters increase.

4. CONCLUSIONS

Turnover rates for H_2O_2 and H_2O formation were measured on silica-supported Pd clusters over a wide range of H_2 and O_2 pressures, and solvent H^+ concentrations in the absence of artifacts from mass transport and secondary decomposition of H_2O_2. These rates were interpreted in order to evaluate the mechanism of direct synthesis. Experiments in solvents with varying H^+ concentrations (including aprotic solvents) demonstrated that protons are essential for H_2O_2 formation, whereas the identity of the counterion is much less important. The dependence of rates on H_2 and O_2 pressures were inconsistent with Langmuirian mechanisms and instead provided evidence for heterolytic reaction pathways similar to the two-electron ORR. Together, these data and their interpretations provided a complete mechanistic understanding of the direct synthesis of H_2O_2 that is consistent with the data and implicates proton−electron transfer elementary steps to form H_2O_2 and O−O bond scission in OOH** to form H_2O. Calculated values for $\Delta H^{\ddagger}$ and $\Delta S^{\ddagger}$ from measured H_2O_2 and H_2O formation rates at varying temperatures show that H_2O formation is more sensitive to the surface electronic structure than is H_2O_2; therefore, selectivity can be increased by increasing the ratio of coordinated to undercoordinated surface atoms. Overall, these results can aid the rational design of inexpensive catalysts that can selectively produce H_2O_2 by direct synthesis in an environmentally benign manner.

■ ASSOCIATED CONTENT

Supporting Information

The Supporting Information is available free of charge on the ACS Publications website at DOI: 10.1021/jacs.5b10669.

TEM images and cluster size distributions of Pd catalysts, procedures used to avoid mass-transport limitations and artifacts from secondary decomposition of H_2O_2, additional rate expressions and their associated derivations, plots showing H_2O turnover rates as a function of [H^+], and formation rates and selectivities for 3 and 7 nm Pd clusters. (PDF)

■ AUTHOR INFORMATION

Corresponding Author

*Phone: (217) 244-2816. Email: dwflhrty@illinois.edu.

DOI: 10.1021/jacs.5b10669
J. Am. Chem. Soc. 2016, 138, 574−586

Notes

The authors declare no competing financial interest.

■ ACKNOWLEDGMENTS

We gratefully acknowledge Mr. Luke Greenfield, Ms. Rong Jiao, and Ms. Christine Rovani for their help synthesizing catalysts and collecting and analyzing rate data. D.W.F. acknowledges Drs. Damien Guironnet and Prashant Jain for their helpful discussions and feedback. Partial financial support for this work was provided by a departmental graduate student fellowship, funded by the Dow Chemical Company. This work was carried out in part in the Frederick Seitz Materials Research Laboratory Central Research Facilities, University of Illinois. Cover Art by Imaging Technology Group, Beckman Institute, University of Illinois.

■ REFERENCES

(1) Hydrogen Peroxide. In *Ullmann's Encyclopedia of Industrial Chemistry*; Wiley-VCH: Weinheim, Germany, 2012; Vol. *18*, pp 393−427.
(2) *EPA Fact Sheet- The Pulp and Paper Industry, the Pulping Process, and Pollutant Releases to the Environment*; Technical Report EPA-821-F-97-011 prepared for U.S. Environmental Protection Agency (EPA), Office of Water: Washington, DC, 1997.
(3) Paper and Pulp. In *Ullmann's Encyclopedia of Industrial Chemistry*; Wiley-VCH: Weinheim, Germany, 2005.
(4) Campos-Martin, J. M.; Blanco-Brieva, G. B.; Fierro, J. L. G. *Angew. Chem., Int. Ed.* **2006**, *45*, 6962.
(5) Samanta, C. *Appl. Catal., A* **2008**, *350*, 133.
(6) Centi, G.; Perathoner, S.; Abate, S. In *Modern Heterogeneous Oxidation Catalysis: Design, Reactions, and Characterization*; Mizuno, N., Ed.; Wiley-VCH Verlag GmbH & Co. KGaA: Weinheim, Germany, 2009; pp 253−287.
(7) Dissanayake, D. P.; Lunsford, J. H. *J. Catal.* **2003**, *214*, 113.
(8) Landon, P.; Collier, P. J.; Carley, A. F.; Chadwick, D.; Papworth, A. J.; Burrows, A.; Kiely, C. J.; Hutchings, G. J. *Phys. Chem. Chem. Phys.* **2003**, *5*, 1917.
(9) Liu, Q.; Bauer, J. C.; Schaak, R. E.; Lunsford, J. H. *Angew. Chem., Int. Ed.* **2008**, *47*, 6221.
(10) Ford, D. C.; Nilekar, A. U.; Xu, Y.; Mavrikakis, M. *Surf. Sci.* **2010**, *604*, 1565.
(11) Todorovic, R.; Meyer, R. J. *Catal. Today* **2011**, *160*, 242.
(12) Lunsford, J. H. *J. Catal.* **2003**, *216*, 455.
(13) Ham, H. C.; Stephens, J. A.; Hwang, G. S.; Han, J.; Nam, S. W.; Lim, T. H. *Catal. Today* **2011**, *165*, 138.
(14) Liu, Q.; Bauer, J. C.; Schaak, R. E.; Lunsford, J. H. *Appl. Catal., A* **2008**, *339*, 130.
(15) Han, Y.-F.; Zhong, Z.; Ramesh, K.; Chen, F.; Chen, L.; White, T.; Tay, Q.; Yaakub, S. N.; Wang, Z. *J. Phys. Chem. C* **2007**, *111*, 8410.
(16) Edwards, J. K.; Thomas, A.; Carley, A. F.; Herzing, A. A.; Kiely, C. J.; Hutchings, G. J. *Green Chem.* **2008**, *10*, 388.
(17) Biasi, P.; Canu, P.; Menegazzo, F.; Pinna, F.; Salmi, T. O. *Ind. Eng. Chem. Res.* **2012**, *51*, 8883.
(18) Edwards, J. K.; Hutchings, G. J. *Angew. Chem., Int. Ed.* **2008**, *47*, 9192.
(19) Edwards, J. K.; Solsona, B.; Ntainjua, E. N.; Carley, A. F.; Herzing, A. A.; Kiely, C. J.; Hutchings, G. J. *Science* **2009**, *323*, 1037.
(20) Biasi, P.; Menegazzo, F.; Pinna, F.; Eranen, K.; Canu, P.; Salmi, T. O. *Ind. Eng. Chem. Res.* **2010**, *49*, 10627.
(21) Liu, Q.; Lunsford, J. H. *Appl. Catal., A* **2006**, *314*, 94.
(22) Ntainjua N., E.; Piccinini, M.; Pritchard, J. C.; Edwards, J. K.; Carley, A. F.; Moulijn, J. A.; Hutchings, G. J. *ChemSusChem* **2009**, *2*, 575.
(23) Deguchi, T.; Iwamoto, M. *J. Catal.* **2011**, *280*, 239.
(24) Choudhary, V. R.; Samanta, C. *J. Catal.* **2006**, *238*, 28.
(25) Choudhary, V. R.; Samanta, C.; Gaikwad, A. G. *Chem. Commun.* **2004**, 2054.
(26) Menegazzo, F.; Signoretto, M.; Frison, G.; Pinna, F.; Strukul, G.; Manzoli, M.; Boccuzzi, F. *J. Catal.* **2012**, *290*, 143.
(27) Kim, S.; Lee, D.-W.; Lee, K.-Y.; Cho, E. A. *Catal. Lett.* **2014**, *144*, 905.
(28) Abate, S.; Centi, G.; Melada, S.; Perathoner, S.; Pinna, F.; Strukul, G. *Catal. Today* **2005**, *104*, 323.
(29) Krishnan, V. V.; Dokoutchaev, A. G.; Thompson, M. E. *J. Catal.* **2000**, *196*, 366.
(30) Burch, R.; Ellis, P. R. *Appl. Catal., B* **2003**, *42*, 203.
(31) Hohenegger, M.; Bechtold, E.; Schennach, R. *Surf. Sci.* **1998**, *412-413*, 184.
(32) Chorkendorff, I.; Niemantsverdriet, J. W. *Concepts of Modern Catalysis and Kinetics*, 2nd ed.; Wiley-VCH: Weinheim, Germany, 2007.
(33) Erley, W. *Surf. Sci.* **1982**, *114*, 47.
(34) Erley, W. *Surf. Sci.* **1980**, *94*, 281.
(35) Fukushima, T.; Song, M.-B.; Ito, M. *Surf. Sci.* **2000**, *464*, 193.
(36) Han, Y.-F.; Lunsford, J. H. *J. Catal.* **2005**, *230*, 313.
(37) Song, C.; Zhang, J. In *PEM Fuel Cell Electrocatalysts and Catalyst Layers*; Zhang, J., Ed.; Springer-Verlag: Vancouver, BC, Canada, 2008; pp 89−134.
(38) Jiao, L.; Regalbuto, J. R. *J. Catal.* **2008**, *260*, 329.
(39) Fagherazzi, G.; Benedetti, A.; Polizzi, S.; Di Mario, A.; Pinna, F.; Signoretto, M.; Pernicone, N. *Catal. Lett.* **1995**, *32*, 293.
(40) Canton, P.; Fagherazzi, G.; Battagliarin, M.; Menegazzo, F.; Pinna, F.; Pernicone, N. *Langmuir* **2002**, *18*, 6530.
(41) *Safety Standard for Hydrogen and Hydrogen Systems: Guidelines for Hydrogen System Design, Materials Selection, Operations, Storage, and Transportation*; NSS 1740.16, prepared for National Aeronautics and Space Administration (NASA), Office of Safety and Mission Assurance: Washington DC, 1997.
(42) Baga, A. N.; Johnson, G. R. A.; Nazhat, N. B.; Saadalla-Nazhat, R. A. *Anal. Chim. Acta* **1988**, *204*, 349.
(43) Madon, R. J.; Boudart, M. *Ind. Eng. Chem. Fundam.* **1982**, *21*, 438.
(44) Hibbitts, D. D.; Neurock, M. *J. Catal.* **2013**, *299*, 261.
(45) Yeh, K.-Y.; Wasileski, S. A.; Janik, M. J. *Phys. Chem. Chem. Phys.* **2009**, *11*, 10108.
(46) Keith, J. A.; Jacob, T. *Angew. Chem., Int. Ed.* **2010**, *49*, 9521.
(47) Voloshin, Y.; Halder, R.; Lawal, A. *Catal. Today* **2007**, *125*, 40.
(48) Kunimatsu, K.; Yoda, T.; Tryk, D. A.; Uchida, H.; Watanabe, M. *Phys. Chem. Chem. Phys.* **2010**, *12*, 621.
(49) Anderson, A. B. *Electrochim. Acta* **2002**, *47*, 3759.
(50) Marković, N. M.; Gasteiger, H. A.; Grgur, B. N.; Ross, P. N. *J. Electroanal. Chem.* **1999**, *467*, 157.
(51) Grgur, B. N.; Marković, N. M.; Ross, P. N. *Can. J. Chem.* **1997**, *75*, 1465.
(52) Karlberg, G. S. *Phys. Rev. B: Condens. Matter Mater. Phys.* **2006**, *74*, 153414.
(53) Dean, J. A. *Lange's Handbook of Chemistry*, 15th ed.; McGraw-Hill, Inc.: New York, 1999.
(54) Shi, L.; Goldbach, A.; Zeng, G.; Xu, H. *Catal. Today* **2010**, *156*, 118.
(55) Guo, X.; Hoffman, A.; Yates, J. T., Jr. *J. Chem. Phys.* **1989**, *90*, 5787.
(56) Johansson, M.; Skúlason, E.; Nielsen, G.; Murphy, S.; Nielsen, R. M.; Chorkendorff, I. *Surf. Sci.* **2010**, *604*, 718.
(57) Li, J.; Yoshizawa, K. *Catal. Today* **2015**, *248*, 142.
(58) Ham, H. C.; Hwang, G. S.; Han, J.; Nam, S. W.; Lim, T. H. *J. Phys. Chem. C* **2010**, *114*, 14922.
(59) Keith, J. A.; Jerkiewicz, G.; Jacob, T. *ChemPhysChem* **2010**, *11*, 2779.
(60) McMillen, D. F.; Golden, D. M. *Annu. Rev. Phys. Chem.* **1982**, *33*, 493.
(61) Wang, Y.; Balbuena, P. B. *J. Chem. Theory Comput.* **2005**, *1*, 935.
(62) Jacob, T. *Fuel Cells* **2006**, *6*, 159.
(63) Voloshin, Y.; Lawal, A. *Chem. Eng. Sci.* **2010**, *65*, 1028.
(64) Choudhary, V. R.; Samanta, C.; Jana, P. *Method for production of hydrogen peroxide with improved yield and selectivity by direct oxidation of hydrogen over palladium containing catalyst*. U.S. Patent 7,288,240, October 30, 2007.
(65) Keith, J. A.; Jacob, T. In *Theory and Experiment in Electrocatalysis*, 50th ed.; Balbuena, P. B., Subramanian, V. R., Eds.; Springer: New York, 2010; pp 89−132.

DOI: 10.1021/jacs.5b10669
J. Am. Chem. Soc. 2016, 138, 574−586

(66) Gao, F.; Wang, Y.; Goodman, D. W. *J. Am. Chem. Soc.* **2009**, *131*, 5734.
(67) Marković, N. M.; Ross, P. N. *Surf. Sci. Rep.* **2002**, *45*, 117.
(68) Faguy, P. W.; Markovic, N.; Adzic, R. R.; Fierro, C. A.; Yeager, E. B. *J. Electroanal. Chem. Interfacial Electrochem.* **1990**, *289*, 245.
(69) Lucas, C. A.; Marković, N. M.; Ross, P. N. *Phys. Rev. B: Condens. Matter Mater. Phys.* **1997**, *55*, 7964.
(70) García-Serna, J.; Moreno, T.; Biasi, P.; Cocero, M. J.; Mikkola, J.-P.; Salmi, T. O. *Green Chem.* **2014**, *16*, 2320.
(71) Hâncu, D.; Beckman, E. J. *Green Chem.* **2001**, *3*, 80.
(72) Anslyn, E. V.; Dougherty, D. A. *Modern Physical Organic Chemistry*; University Science Books: Sausalito, CA, 2006.
(73) Janik, M. J.; Taylor, C. D.; Neurock, M. *J. Electrochem. Soc.* **2009**, *156*, B126.
(74) Ou, L.; Yang, F.; Liu, Y.; Chen, S. *J. Phys. Chem. C* **2009**, *113*, 20657.
(75) Anderson, A. B.; Roques, J.; Mukerjee, S.; Murthi, V. S.; Marković, N. M.; Stamenkovic, V. *J. Phys. Chem. B* **2005**, *109*, 1198.
(76) Khan, A.; Lu, X.; Aldous, L.; Zhao, C. *J. Phys. Chem. C* **2013**, *117*, 18334.
(77) Tang, W.; Lin, H.; Kleiman-Shwarsctein, A.; Stucky, G. D.; McFarland, E. W. *J. Phys. Chem. C* **2008**, *112*, 10515.
(78) van Hardeveld, R.; Hartog, F. *Surf. Sci.* **1969**, *15*, 189.
(79) Kolasinski, K. W.; Cemic, F.; Hasselbrink, E. *Chem. Phys. Lett.* **1994**, *219*, 113.
(80) Nolan, P. D.; Lutz, B. R.; Tanaka, P. L.; Mullins, C. B. *Surf. Sci.* **1998**, *419*, L107.
(81) Nyberg, C.; Tengstal, C. G. *Surf. Sci.* **1983**, *126*, 163.
(82) Stuve, E. M.; Madix, R. J.; Brundle, C. R. *Surf. Sci.* **1984**, *146*, 155.
(83) Junell, P.; Honkala, K.; Hirsimaki, M.; Valden, M.; Laasonen, K. *Surf. Sci.* **2003**, *546*, L797.
(84) Burgess, D. R. In *NIST Chemistry WebBook, NIST Standard Reference Database Number 69*; Linstrom, P. J., Mallard, W. G., Eds.; National Institute of Standards and Technology: Gaithersburg, MD, 2015. http://webbook.nist.gov (accessed on November 18, 2015).
(85) Ben-Naim, A.; Marcus, Y. *J. Chem. Phys.* **1984**, *81*, 2016.
(86) Chandler, D. *Nature* **2005**, *437*, 640.

DOI: 10.1021/jacs.5b10669
J. Am. Chem. Soc. 2016, 138, 574−586